Due consideration of the breakup and direct reaction mechanisms within (d, p), $(d, 2p)$, $(d, xn2p)$, and (d, xn) reactions

Marilena Avrigeanu[1,*] and *Vlad* Avrigeanu[1,**]

[1]Horia Hulubei National Institute for Physics and Nuclear Engineering, P.O. Box MG-6, 077125 Bucharest-Magurele, Romania

Abstract. Suitable account of available excitation-function of deuterons interaction with target nuclei components of candidates materials for the ITER fusion reactor, the European DEMO fusion reactor, and the IFMIF-DONES Irradiation Facility has been proved by consistent analysis of the reaction mechanisms involved in the complex deuteron-nucleus interaction. In this work the attention has been focused on the analysis of the deuteron activation cross sections related to the gas accumulation, (d, p), $(d, 2p)$, $(d, xn2p)$, and to the strong neutron emission, (d, xn), interaction processes of interest for the radiation damage and shielding design studies devoted to the structural materials selection. The key role of direct interactions, i.e., breakup, stripping and pick-up processes is stressed out by the comparison of data with theoretical and evaluation predictions.

1 Introduction

The interest in deuteron interaction process is the result of high accuracy deuteron nuclear data request coming from the large international projects ITER, Fusion Materials Irradiation Facility (IFMIF), SPIRAL2 and SARAF accelerators [1], as well as from medical investigations using deuterons beam. Complementary, research programmes devoted to the update of both the experimental nuclear data systematics and the theoretical frame of the data analysis have been started as FENDL library and EURATOM EUROfusion [2].

Increased attention should be focused in this respect on the deuteron nuclear data assessment which are very modest compared with the neutron one, while even the newest evaluations show apparent discrepancies with the scarce measurements. These discrepancies between the data and either theoretical or evaluated predictions stress out neglected peculiarity of the deuteron interactions which make substantially different the deuteron-projectile among the other incident particles.

2 Nuclear reaction models analysis

The specific reaction mechanism of deuteron interactions is the deuteron breakup (BU). Its complexity is given also by the supplementary nuclear reactions initiated by the nucleons following the deuteron breakup [3, 4]. In addition to the breakup mechanism, the deuteron

*e-mail: marilena.avrigeanu@nipne.ro
**e-mail: vlad.avrigeanu@nipne.ro

interactions involve largely the direct reactions (DR) of stripping, (d, n) and (d, p), and pick-up (d, t), $(d,^3 He)$, and (d, α). Therefore, the direct interactions (DI), as the sum of BU and DR mechanisms, complete the picture of the complex deuteron interactions, so far considered as the result of only statistical mechanisms, i.e. the pre-equilibrium emission (PE) and fully equilibrated compound–nucleus (CN) decay.

2.1 Deuteron breakup

Details concerning the physical picture of the deuteron breakup in the Coulomb and nuclear fields of the target nucleus were given recently [3, 4]. Accordingly, only particular points are mentioned hereafter for the distinct processes that are considered in this respect, namely the elastic breakup (EB) in which the target nucleus remains in its ground state and none of the deuteron constituents interacts with it, and the inelastic breakup or breakup fusion (BF), where one of these deuteron constituents interacts nonelastically with the target nucleus.

The deuteron breakup parametrization within Ref.[3] has concerned the dependence on deuteron incident energy E as well as target–nucleus atomic (Z) and mass (A) numbers, of the ratios of elastic and total breakup proton–emission cross sections σ_{EB}/σ_R and σ^p_{BU}/σ_R, respectively, to the deuteron reaction cross section σ_R:

$$\sigma^p_{BU}/\sigma_R = 0.087 - 0.0066Z + 0.00163ZA^{1/3} + 0.0017A^{1/3}E - 0.000002ZE^2 \quad , \tag{1}$$

$$\sigma_{EB}/\sigma_R = 0.031 - 0.0028Z + 0.00051ZA^{1/3} + 0.0005A^{1/3}E - 0.000001ZE^2 \quad , \tag{2}$$

Then, the usual assumption that BF nucleon–emission cross sections σ^n_{BF} and σ^p_{BF} are equal led finally to σ^p_{BF}=σ^p_{BU}-σ_{EB}. More details concerning the extrapolation of σ_{EB} beyond the energy domain of experimental systematic, and the constraint due to scarce data exiting for heaviest target nuclei (A>200) are given elsewhere [3, 4].

The energy dependence of σ_R, σ_{BU}, σ^p_{BU} as well as of its components σ_{EB} and σ^p_{BF} is shown in Fig 1 for deuteron interactions with ^{52}Cr and ^{94}Mo target nuclei. Thus, their variation with target–nucleus mass number is emphasized, too. The BU excitation functions increase with the deuteron-energy increasing, while its dominant BF component is quite important for the analysis of two opposite BU effects on deuteron–activation cross sections, briefly recalled hereinafter.

Firstly, the total-reaction cross section that is shared among different outgoing channels, is reduced by the value of σ_{BU}. On the other hand, the BF component brings additional contributions to different reaction channels of the deuteron-nucleus interaction [4–15]. Thus, interactions of the breakup protons or neutrons with the target nucleus contribute to enhancement of the corresponding (d, xn) or (d, xp) reaction cross sections, respectively. The compound nuclei in breakup-nucleon induced reactions, $(A + 1)_Z$ and $(A + 1)_{Z+1}$, have the A and maybe also Z numbers with one unit smaller than in the case of deuteron–induced reaction, $(A + 2)_{Z+1}$. The partition of the BF cross section among various residual-nuclei population is triggered by the energy spectra of the breakup nucleons and the excitation functions of the reactions induced by these nucleons on the target nuclei [3, 4].

In order to calculate the BF enhancement of, e.g., (d, xn) reaction cross sections, the BF proton–emission cross sections σ^p_{BF} should be (i) multiplied by the proton enhancing ratios $\sigma_{(p,x)}/\sigma^p_R$, (ii) convoluted with the Gaussian line shape distribution of the breakup–proton

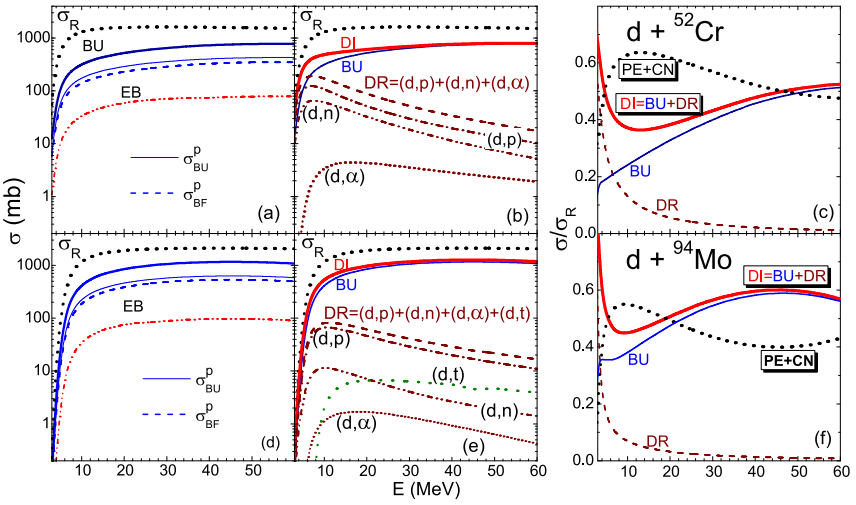

Figure 1. Excitation functions of (a,b,d,e) deuteron total–reaction σ_R (thick dotted curves), (a,d) total–breakup σ_{BU} (thick solid), total–breakup *nucleon*–emission σ^p_{BU} (thin solid), inelastic–breakup *nucleon*–emission σ^p_{BF} (dashed–dotted), and elastic–breakup σ_{EB} (dash-dot-dotted) [3], (b,e) DI excitation functions (thick solid curves) and its components: total BU (thin solid curves), DR (dashed curves), stripping (d, p) (dash-dotted curves) and (d, n) (dash-dot-dotted curves), and pick-up (d, α) (short-dotted curves) and (d, t) (dotted curve), and (c,f) σ_R fractions of BU (thin solid curves), DR (dashed curves), DI (thick solid curves), and PE+CN (dotted curves) cross sections of deuteron interactions with ^{52}Cr and ^{94}Mo nuclei, respectively (see text).

energy E_p for a given deuteron incident energy E, and (iii) integrated over the breakup–proton energy. Consequently, the BF–enhancement cross sections have the form [4, 7–10, 12]:

$$\sigma^{p,x}_{BF}(E) = \sigma^{p}_{BF}(E) \int_0^{E^{max}_{BU}} dE_p \ \frac{\sigma_{(p,x)}(E_p)}{\sigma^p_R} \times \frac{1}{(2\pi)^{\frac{1}{2}} w} exp[-\frac{(E_p - E^0_p(E))^2}{2w^2}] \ , \quad (3)$$

where σ^p_R is the proton total–reaction cross section, x stands for various γ, n, d, or α outgoing channels, while w and E^0_p are the Gaussian distribution parameters given by Kalbach [16]. E^{max}_{BU} is the maximum energy of the breakup nucleon, i.e. the difference between the deuteron incident energy and its binding energy B_d [3, 4]. Interpolation of nucleon–induced reaction cross sections, available either experimentally [17] or through TENDL [18] evaluated–data library, has been involved within estimation of the nucleon–enhancing ratios [4–14]. Thus, the supplementary uncertainties brought by additional theoretical calculations there have been reduced as much as possible.

The above–mentioned BU cross–section parametrization as well as the inelastic–breakup enhancement are included in TALYS-1.96 code [19], and selected by the option *breakup-model* keyword value 2.

The BF enhancements, brought by breakup–nucleons interactions with target nuclei, are important mainly for describing the excitation functions for second– and third–chance particle emission within the deuteron–induced reactions. This is shown in Figs. 3(e), 4(a,b), and 5(b,c,d,g,h) of Sec. 3.

2.2 Direct reactions

The deuteron interaction with low- and medium-mass target nuclei, at incident energies below and around the Coulomb barrier, proceeds largely through stripping (d,p) and (d,n), and pick-up (d,t), $(d,^3He)$, and (d,α) DR reactions. While usually the reaction Q-values for (d,p) and (d,n) reactions are positive, the distinct separation of the breakup and stripping mechanisms is done by the maximum energy limit for breakup nucleon emission, actually the *breakup threshold*, given by the energies difference $E\text{-}B_d$.

The model calculation of the stripping and pickup DR contributions, not included within TALYS code [19], has been performed using the distorted-wave Born approximation (DWBA) model within the code FRESCO [20]. The post/prior form distorted-wave transition amplitudes for $(d,n/p)$ stripping and respectively $(d,t/^3He/\alpha)$ pickup reactions, as well as the finite–range interaction have been considered. The n-p effective interaction in deuteron [21], d-n interaction in the triton [22], as well as d-p interaction in ^{3}He [23], are assumed to have a Gaussian shape, at the same time with a Woods-Saxon shape [24] of the d-d effective interaction in the α particle. The transferred-nucleon bound states were generated in a Woods-Saxon real potential [5–13].

The number of N nodes corresponding to an L transferred angular momentum in the radial wave function was determined by the harmonic–oscillator energy conservation rule:

$$2N + L = 2(n_{n/p} - 1) + l_{n/p}, \tag{4}$$

where $n_{n/p}$ and $l_{n/p}$ are the single–particle (neutron/proton) shell–model state quantum numbers. Particularly for the FRESCO code, the number of nodes includes the origin, so that N>0.

The populated discrete levels and the corresponding spectroscopic factors available within the ENSDF library [25] were used as starting input for the DWBA stripping and pick-up excitation functions calculation. Further analysis of the measured outgoing particles angular distributions has provided the ultimate spectroscopic factors for transitions to discrete levels of residual nuclei, and the related DR cross sections, as presented in Fig. 1(b,e).

The DR contributions are important for describing the measured excitation functions corresponding to the first–chance particle emission, as shown by dash-dotted curves in Figs. 2(b,d), 3(b,d), and 5(c,f) in Sec. 3.

It should be stressed that the transfer reactions contributions to various residual nuclei population are relevant at low incident energies. Then, their excitation functions decrease with the deuteron energy increase. At the same time, the BU excitation function is still increasing with the incident energy, leading to the same trend of the DI excitation function shown in Fig. 1(b,e).

Finally, the appropriate account of the deuteron incident–flux decrease due to its absorption within BU and DR processes provides the corrected total–reaction cross section going towards PE+CN statistical decay of the excited system. Thus, a reduction factor of the deuteron σ_R due to the incident flux leakage through DI accounted in the present analysis is given by:

$$1 - \frac{\sigma_{BU} + \sigma_{DR}}{\sigma_R} = 1 - \frac{\sigma_{DI}}{\sigma_R} = \frac{\sigma_{PE} + \sigma_{CN}}{\sigma_R}. \tag{5}$$

Its energy dependence is shown in Fig. 1(c,f) for deuteron interaction with with ^{52}Cr and ^{94}Mo target nuclei, respectively, together with the fractions to σ_R of the DI cross section and its BU and DR components. First, one may note the high importance of the ratio σ_{DI}/σ_R at the lowest incident energies, due to the above-mentioned behavior of the DR excitation function. On the other hand, the decrease of the DR component leads to a steep increase of the PE+CN weight with the deuteron energy, while the BU increase is much lower than the

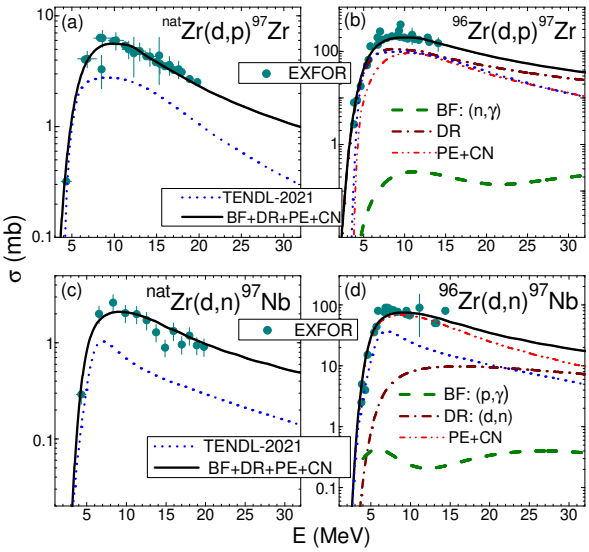

Figure 2. (Color online) Comparative analysis of the reaction mechanisms involved in the first–chance particle emission (d, p) and (d, n) reactions: (a) ^{nat}Zr$(d, p)^{97}$Zr, (b) ^{96}Zr$(d, p)^{97}$Zr, (c) ^{nat}Zr$(d, n)^{97}$Nb, and (d) ^{96}Zr$(d, n)^{97}$Nb, along with TENDL–2021 evaluation [18] (short dashed curves), and model calculations (solid curves) including BF enhancements (dashed), stripping (d, p) and (d, n) reactions (dash-dotted), and PE+CN components corrected for DI deuteron–flux leakage (dash-dot-dotted) (see text).

same trend of σ_R. Next, the PE+CN fraction reaches its maximum at the deuteron energies of 15–20 MeV, and continues with a slow decrease due to the continuous BU increase with the incident energy.

Overall, along the actual incident energy range up to 60 MeV, the DI and PE+CN components have values around half of σ_R [7, 9, 10, 12], pointing out the quite important role of the so far neglected direct interactions.

2.3 Statistical emission

The pre-equilibrium emission and decay of the fully-equilibrated compound nucleus become important with the increase of the incident energy above the Coulomb barrier (e.g., Ref. [3]). The corresponding reaction cross sections have been calculated using the TALYS code [19] taking into account also the above–discussed BU approach as well as the stripping and pick–up reaction mechanisms through the reduction factor of the deuteron reaction cross section, of Eq. (5).

The following input options of the TALYS code have been used: (a) the OMPs of Koning-Delaroche [26], Daehnick *et al.* [27], Becchetti-Greenlees [28], and Avrigeanu *et al.* [29, 30] for neutrons and protons, deuterons, tritons, and α-particles, respectively, (b) the back-shifted Fermi gas (BSFG) formula for the nuclear level density, and (c) the pre-equilibrium spin distribution of the particle-hole state densities.

An important issue of the model calculations is the use of the same model parameters to account for different reaction mechanisms as, e.g., the same OMP parameters for calculation of the distorted waves in the ingoing/outgoing channels of direct reactions, the PE transition rates, and the transmission coefficients of various CN channels.

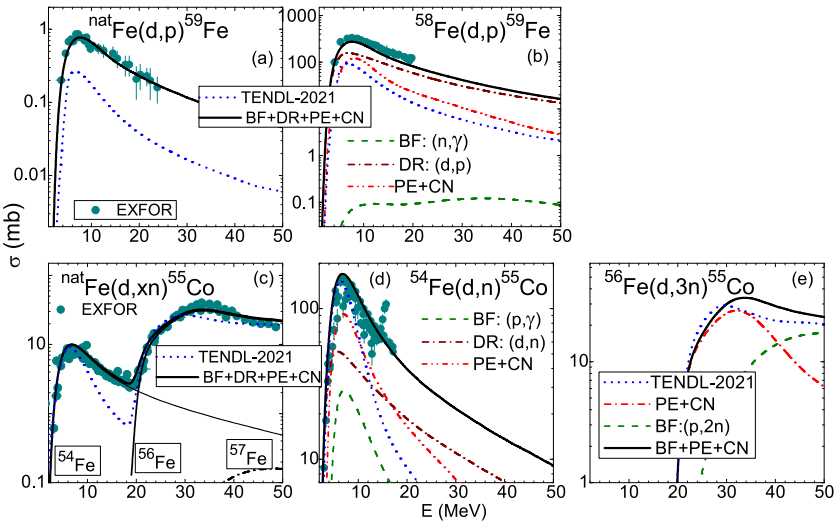

Figure 3. (Color online) Comparative analysis of the reaction mechanisms involved in the (d, p) and (d, xn) reactions, i.e. (a) ^{nat}Fe$(d, p)^{59}$Fe, (b) ^{58}Fe$(d, p)^{59}$Fe, (c) ^{nat}Fe$(d, xn)^{55}$Co, (d) ^{54}Fe$(d, n)^{55}$Co, and (e) ^{56}Fe$(d, 2n)^{55}$Co, along with TENDL–2021 evaluation [18] (short dashed curves), and model calculations (solid curves) including BF enhancements (dashed curves), stripping (d, p) as well as (d, n) reactions (dash-dotted curves), and PE+CN components corrected for DI deuteron flux leakage (dash-dot-dotted curves). (c) Contributions of *Fe* isotopes through (d, n), $(d, 3n)$, and $(d, 4n)$ reactions to ^{55}Co activation are also shown (thin, dashed, and dash-dotted curves, respectively) (see text).

3 Reaction mechanism competition within (d, p), (d, xn), and $(d, xn2p)$ reactions

The accurate description of the protons, tritons, and helium–particles emission in deuteron induced reactions is very important for the radiation damage studies, e.g. of the bubble gas accumulation at the surface of the materials. On the other hand, the estimation of the complementary strong neutron emission is essential for radiation damage studies, too, but also to diminish the radioactive risk through the adequate shielding design. Therefore, the present analysis of proton and neutron emission in deuteron induced reactions is devoted to the target nuclei common in the alloys of candidate materials for ITER and IFMIF installations [1] as the stable isotopes of Cr, Mn, Fe, Co, Ni, Cu, Zr, Nb, and Mo elements [6–13]. A consistent account of *BU* and *DR* reaction mechanism contributions seems essential in this respect due to the still existing disagreement between measurements and evaluated data, the weak points of an evaluation procedure being carefully analized too.

3.1 (d, p), (d, n), and (d, xn) reactions

The analysis of ^{97}Zr and ^{97}Nb residual–nuclei activation by deuterons incident on ^{nat}Zr target involves actually only the neutron–richest stable isotope ^{96}Zr. It is completed, actually quite rarely, by the measurements of the similar excitation functions [17] corresponding to the deuterons interacting with this isotope, i.e. ^{96}Zr$(d, p)^{97}$Nb and ^{96}Zr$(d, n)^{97}$Zr (Fig. 2). The suitable description of the measured excitation functions [17] of ^{97}Zr activation by deuterons incident on either ^{nat}Zr or ^{96}Zr [Fig. 2(a,b)] stands particularly for a distinct test of the present

model approach due to the involvement of the breakup, stripping, and PE+CN reaction mechanisms.

For the first–chance particle emission reaction (d, p), the DR stripping mechanism prevails over the statistical PE+CN especially at the lowest deuteron energies, below ∼10 MeV, as well as above 20 MeV. Comparatively, the inelastic breakup enhancement contribution brought by the breakup neutrons through ^{96}Zr$(n, \gamma)^{97}$Zr reaction is lower by two orders of magnitudes. The effect of neglecting the important role of DR stripping process in the (d, p) reaction is illustrated by the evaluated TENDL underestimation of both ^{nat}Zr$(d, p)^{97}$Zr and ^{96}Zr$(d, p)^{97}$Zr reaction data. Actually, this proof is just in line with the previous discussion of the experimental (d, p) excitation functions for ^{51}V [6], ^{50}Cr [7], ^{55}Mn [8], ^{59}Co [6], ^{64}Ni [10], ^{93}Nb [13], and ^{96}Zr [12] target nuclei, which could not be described as long as the strong stripping (d, p) contribution was neglected.

Comparison of the above (d, p) reaction analysis with the description of the measured ^{nat}Zr$(d, n)^{97}$Nb and ^{96}Zr$(d, n)^{97}$Nb excitation functions [17] stress the dominant role of the statistical PE+CN emission as well as an important contribution of stripping reaction (d, n). On the other hand, as for the (d, p) reaction, the BF enhancement brought by the breakup protons through (p, γ) reaction is negligible.

The above pointed out specific features of the (d, p) reaction are confirmed also by the analysis of ^{58}Fe$(d, p)^{58}$Fe reaction in Fig. 3(b), where the DR stripping is the dominant reaction mechanism along the whole incident energy interval. Similarly to Fig. 2(b), the inelastic breakup enhancement brought by breakup neutrons through ^{58}Fe$(n, \gamma)^{59}$Fe reaction is lower by two orders of magnitudes. The effect of neglecting the important role of DR stripping process in the (d, p) reaction is illustrated by the underestimation of TENDL evaluation apparent for ^{nat}Fe$(d, p)^{59}$Fe as well as ^{58}Fe$(d, p)^{59}$Fe reaction data.

The account of ^{nat}Fe$(d, xn)^{55}$Co, ^{54}Fe$(d, n)^{55}$Co, and ^{56}Fe$(d, 2n)^{55}$Co reactions, shown in Fig. 3(c,d,e), makes obvious the main role of the statistical PE+CN mechanisms. Nevertheless, important contributions of the stripping reaction, in Fig. 3(d), and inelastic breakup enhancement brought by breakup protons through (p, γ) and $(p, 2n)$ reactions, in Fig. 3(d,e), have been evidenced too. Therefore, the apparent discrepancy of evaluation predictions and measured ^{54}Fe$(d, n)^{55}$Co excitation function in Fig. 3(d) could be considered to follow the oversight of the DI, stripping (d, n), and BF (p, γ) reactions contributions.

The role of stripping (d, n) and BF enhancement of (p, γ) reactions is shown once more in Fig. 3(c), less spectacular than for (d, p) reactions but still important, by a comparative analysis of the measured [17], model calculations, and evaluation predictions [18] of ^{nat}Fe$(d, xn)^{55}$Co excitation function. Actually, the ^{54}Fe$(d, n)^{55}$Co reaction is the only one responsible for ^{58}Co activation at incident energies up to ∼20MeV, as a result of the reaction thresholds for the corresponding contributions of the heavier Fe isotopes (e.g., E_{th}=18.3 MeV for ^{56}Fe$(d, 3n)^{55}$Co reaction). Consequently, the effects of the (d, n) stripping and (p, γ) breakup enhancement contributions, beyond the TENDL evaluation, are most clearly viewed in the absence of strong addition coming above 20 MeV from the most abundant ^{56}Fe isotope.

Overall, it could be considered that the present account of measured (d, p), (d, n), and (d, xn) activation excitation functions validates the underlined theoretical frame, highlighting the role of stripping mechanism within the first–chance particle emission reactions.

3.2 $(d, 2p)$, $(d, xn2p)$, and (d, xn) reactions

Comparative analysis of either the (d, p) and (d, n), or $(d, 2p)$ and $(d, 2n)$ reactions in Fig. 2(b,d) and Fig. 4(a,b), respectively, evidences the well increased importance of the inelastic breakup enhancement for the second–chance particle emission cross sections. Thus, while there is a negligible BF enhancement to the (d, p) reaction, brought by breakup–neutron

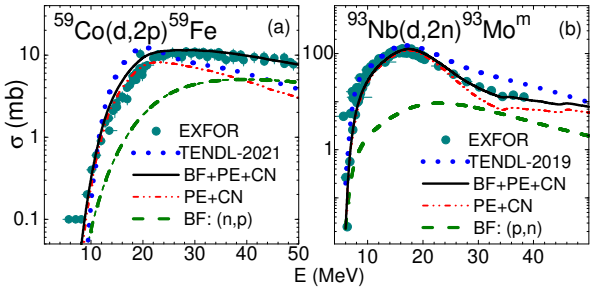

Figure 4. (Color online) Comparative analysis of the reaction mechanisms involved in the second–chance particle emission within (a) ^{59}Co$(d,2p)^{59}$Fe and (b) ^{93}Nb$(d,2n)^{93}$Mo^m reactions, along with TENDL-2021 evaluation [18] (short dashed curves) and model calculations (solid curves) including BF enhancements (dashed) and PE+CN components corrected for DI deuteron flux leakage (dash-dot-dotted) (see text).

induced (n,γ) reaction in Fig. 2(b), the BF enhancement to $(d,2p)$ reaction, due to the (n,p) reaction, overcomes the PE+CN excitation function at incident energies above ~35MeV in Fig. 4(a). The same significant importance has the breakup–proton induced (p,n) enhancement to the $(d,2n)$ reaction cross sections in Fig. 4(b), with a contribution comparable to the PE+CN mechanisms for energies over ~30 MeV. Therefore, the account of the measured ^{59}Co$(d,2p)^{59}$Fe and ^{93}Nb$(d,2n)^{93}$Mo^m excitation functions confirm the present theoretical approach taking into consideration particularly the breakup and PE+CN mechanisms contributions.

The analysis of ^{58}Co activation through ^{nat}Ni$(d,xn2p)^{58}$Co reaction shown in Fig. 5(a) points out the notable dominance of ^{58}Ni$(d,2p)$ reaction along the broad incident–energy range of ~8-35 MeV. Similarly as in the above cases, a proper account of ^{58}Ni$(d,2p)^{58}$Co excitation function in Fig. 5(b) has been obtained by addition of the BF enhancement contribution of the breakup–neutron induced (n,p) reaction to the PE+CN mechanisms yield.

However, below the effective threshold of the $(d,2p)$ reaction, i.e. below the incident energy of ~8 MeV, the unique contribution to the ^{58}Co residual nucleus population comes from the ^{60}Ni$(d,2n2p)$ reaction channel shown in Fig. 5(a). Then, the same ^{60}Ni$(d,2n2p)$ reaction provides the strongest contribution to ^{58}Co activation above the incident energy of ~35 MeV. Actually, the excitation function of the population of ^{58}Co residual nucleus through this reaction shows two maxims in Fig. 5(c). The former corresponds to the (d,α) channel which goes also through a DR pick-up process, in addition to the BF and PE+CN mechanisms for completion of ^{60}Ni$(d,2n2p)$ reaction analysis. The latter corresponds to the whole sequential nucleon emission, with higher threshold energies as, e.g., E_{th}=14.7 MeV for (d,n^3He) reaction, than the threshold of (d,α) reaction. However, no maximum of (d,α) excitation function in Fig. 5(c) is distinguishable within ^{nat}Ni$(d,xn2p)^{58}$Co excitation function in Fig. 5(a), due to the overlap of the most abundant ^{58}Ni isotope contribution. While the ^{60}Ni isotope abundance of 26.2% is three times lower, the second maxim of the related $(d,2n2p)$ reaction remains dominant even for ^{nat}Ni$(d,xn2p)^{58}$Co excitation function. Nevertheless, it includes an important BF enhancement that exceeds the pick-up (d,α) contribution over ~35 MeV.

Furthermore, the first maximum of the $(d,3n2p)$ excitation function in Fig. 5(d) includes also the α-particle emission through $(d,p\alpha)$ reaction. The BF corresponding enhancement contribution, consisting mainly in the (p,α) reaction, brings ~10% of this ^{58}Co activation, and enhances the α-particle emission too.

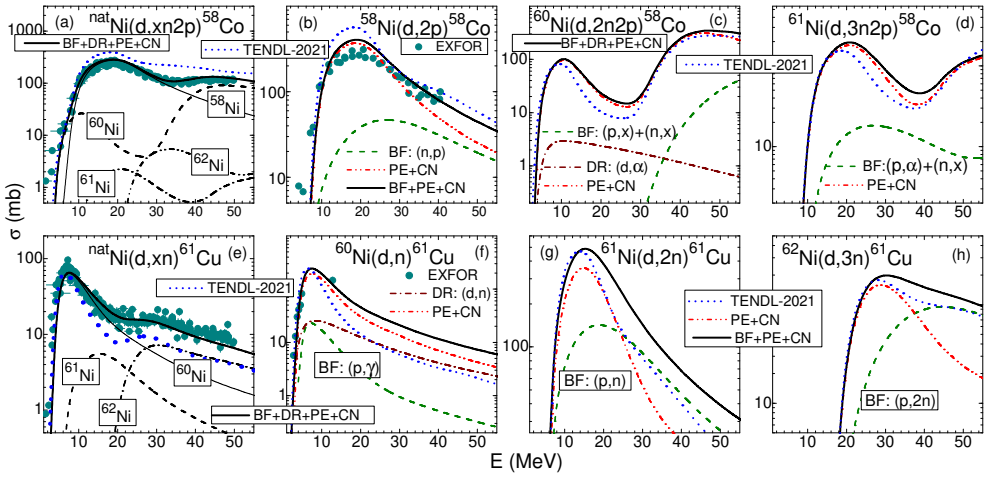

Figure 5. (Color online) Comparative analysis of the reaction mechanisms involved within $(d, xn2p)$ and (d, xn) reactions as (a) ^{nat}Ni$(d, xn2p)^{58}$Co, (b) ^{58}Ni$(d, 2p)^{58}$Co, (c) ^{60}Ni$(d, 2n2p)^{58}$Co, (d) ^{61}Ni$(d, 3n2p)^{58}$Co, and respectively (e) ^{nat}Ni$(d, xn)^{61}$Cu, (f) ^{60}Ni$(d, n)^{61}$Cu, (g) ^{61}Ni$(d, 2n)^{61}$Cu, and (h) ^{62}Ni$(d, 3n)^{61}$Cu, along with TENDL–2021 evaluation [18] (short dashed curves), and model calculations (solid curves) including BF enhancements (dashed curves), pick-up (d, α) and stripping (d, n) reactions (dash-dotted curves), as well as PE+CN components corrected for DI deuteron flux leakage (dash-dot-dotted curves). Contributions of Ni isotopes to either ^{58}Co or ^{61}Cu activation by deuterons incident on ^{nat}Ni are shown (a) for $(d, 2p)$, $(d, 2n2p)$, $(d, 3n2p)$, and $(d, 4n2p)$ reactions (thin, dash, dash-dotted, and dash-dot-dotted curves, respectively), as well as (d) for (d, n), $(d, 2n)$, and $(d, 3n)$ reactions (thin, dash, and dash-dotted curves, respectively) (see text).

Although the ^{62}Ni(d,4n2p)^{58}Co reaction analysis is not detailed in Fig. 5, its contribution to the related activation by deuterons on ^{nat}Ni is shown in Fig. 5(a). It is important for the goal of the present work to point out that the maximum of this excitation function corresponds to the $(d, 2n\alpha)$ reaction on the target nucleus ^{62}Ni.

Finally, the agreement of model calculations with the experimental data as a sound proof of the present consistent consideration of the BU and DR mechanisms, is of particular interest due to $(d, xn2p)$ processes leading to hydrogen and helium gas emission. Thus, it has been relevant to point out their increased importance for the radiation damage studies.

On the other hand, because Ni is a component of stainless steel of interest for nuclear technology, being used as surface coating material too, both charged-particles and neutron emissions are of significant interest. Concerning the strongest neutrons emission in deuteron interaction with ^{nat}Ni target nucleus (Fig. 23 of Ref. [10]), further comments deserve the model calculations including contributions from BU, stripping, and PE+CN mechanisms which describe the measured ^{nat}Ni$(d, xn)^{61}$Cu, and ^{60}Ni$(d, n)^{61}$Cu, Fig. 5(e,f).

The effects of (d, n) stripping and BF enhancement, through breakup–proton induced (p, γ) reaction, are shown by the apparent underestimation of the measured ^{60}Ni(d,n)^{61}Cu excitation function by the evaluation predictions in Fig. 5(f). Thus, the stripping excitation function overcomes the TENDL evaluation above 20 MeV, while the BF enhancement excitation function touches the striping one around ∼10 MeV incident energy, even if then it decreases faster.

Further analysis of the second and third–chance neutron emission residual channels ^{61}Ni(d,2n) and ^{62}Ni$(d, 3n)^{61}$Cu proves the role of BF enhancements brought by breakup pro-

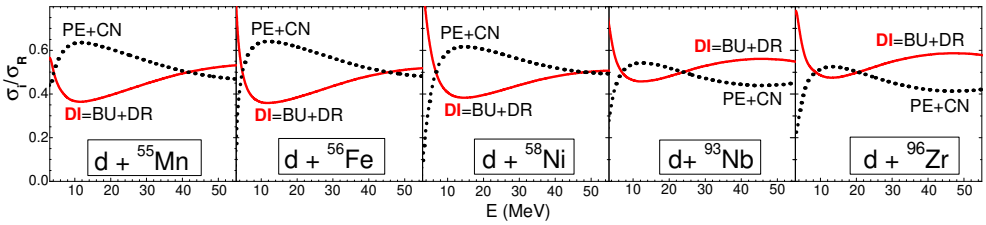

Figure 6. (Color online) The absorption of the incident flux through the main reaction mechanisms of direct interactions DI (solid curves) and statistical emission PE+CN (thick dotted curves), for the deuterons interactions with target nuclei of interest for structural materials: ^{55}Mn, ^{56}Fe, ^{58}Ni, ^{93}Nb, and ^{96}Zr.

tons within ^{61}Ni(p,n) and ^{62}Ni$(p,2n)$ reactions. Their contributions exceed the statistical PE+CN neutron emission yield for deuteron energies higher than ∼30 and ∼40 MeV shown in Fig. 5(g,h), respectively. However, the weak natural abundance of ^{61}Ni isotope (1.14%) leads to the modest $(n,2n)$ contribution to the total activation of ^{61}Cu residual nucleus in Fig. 5(e). Finally, the overlook of above discussed DI contributions is the reason of the apparent underestimation of the measured ^{nat}Ni$(d,xn)^{61}$Cu excitation functions by the evaluation predictions.

4 Conclusions

A detailed theoretical analysis of the reaction mechanisms involved in the hydrogen and helium gas accumulation, as well as in the strong neutron emission has been presented. It has been proved to be necessary for a reliable understanding of the interaction process as well as for assessment of accurate calculated deuteron–activation cross sections.

The most important conclusion of the deuteron interaction process analysis [5, 7–13], pointed out in Fig. 6 too, concerns the key role of direct interactions, i.e. the breakup, stripping, and pickup processes, which absorb around half of the deuteron incident flux.

Moreover, the present theoretical framework has been supported by comparison of the experimental data with the present calculations as well as the corresponding TENDL–2021 evaluation [18]. Distinct discrepancies can be obviously related to the complexity of the interaction process, not entirely accounted for in routine evaluation/theoretical analyzes. As shown in Sec. 3, most of them are due to overlooking the deuteron inelastic–breakup enhancement and appropriate treatment of stripping and pickup processes. This comparative analysis of experimental data, evaluations, and model calculations stress out the weak points and consequently the need for theoretical framework/evaluation upgrade, as well as requirements for new measurements.

At the same time, it could be essential the more recent interest on the microscopic analysis of inclusive breakup and direct reactions [32–34]. While they are still investigated numerically, further progress may contribute eventually to increased accuracy of also the phenomenological evaluation of the deuteron activation. Suitable distinction among the breakup mechanism and the stripping direct reaction within microscopic deuteron breakup will be most beneficial in this respect. The correct assessment of the inelastic breakup enhancement, being triggered by the maximum energy of the breakup nucleon that differs significantly from that of the outgoing stripping nucleons, is thus a prerequisite for semi-classical as well as quantum theories.

Nevertheless, the upgrade of the theoretical frame associated to deuteron interaction processes demands also an overall increase of the deuteron data basis and complementary measurements of either (d, px) and (n, x), or (d, nx) and (p, x) reaction data within corresponding incident-energy ranges. Although the actual scarce data are mainly available for natural elements of structural materials, similar measurements on their distinct isotopes would be most useful for model endorsement. Recent programs at strong new facilities [35, 36] seem really promising.

Actually, the key achievement of the consistent theoretical approach of the deuteron interaction processes, supported by advanced codes associated to the nuclear reaction mechanisms, is especially its predictive power. Therefore, update of the theoretical framework of deuteron-nucleus interaction will improve the evaluation predictions for target nuclei and incident energies where data are still missing but strongly requested by the current engineering design projects.

Acknowledgments

This work has been partly supported by The Executive Unit for the Financing of Higher Education, Research, Development and Innovation (UEFISCDI) (Project No. PN-III-ID-PCE-2021-0642) and carried out within the framework of the EUROfusion Consortium, funded by the European Union via the Euratom Research and Training Programme (Grant Agreement No 101052200 — EUROfusion). Views and opinions expressed are however those of the author(s) only and do not necessarily reflect those of the European Union or the European Commission. Neither the European Union nor the European Commission can be held responsible for them.

References

[1] ITER organization (2007), http://www.iter.org/; www.ifmif.org; www.ganil-spiral2.eu; www.gov.il/en/Departments/publications/reports/facilitysaraf

[2] Fusion Evaluated Nuclear Data Library (FENDL) 3.0; https://www-nds.iaea.org/fendl30/; https://www.instituteforgovernment.org.uk/article/explainer/euratom/; /euro-fusion.org/

[3] M. Avrigeanu, W. von Oertzen, R. A. Forrest *et al.*, Fusion Eng. Design **84**, 418 (2009); M. Avrigeanu and A. M. Moro, Phys. Rev. C **82**, 037601 (2010); M. Avrigeanu and V. Avrigeanu, Phys. Rev. C **92** 021601(R) (2015)

[4] M. Avrigeanu and V. Avrigeanu, Phys. Rev. C **95**, 024607 (2017); M. Avrigeanu, D. Rochman, A.J. Koning *et al.*, Eur. Phys. J. A **58**:3 (2022)

[5] P. Bém, E. Šimečková, M. Honusek *et al.*, Phys. Rev. C **79**, 044610 (2009)

[6] A. Kreisel, L. Weissman , A. Cohen *et al.*, Phys. Rev. C **99**, 034611 (2019)

[7] E. Šimečková, M. Avrigeanu, U. Fischer *et al.*, Phys. Rev. C **98**, 034606 (2018)

[8] M. Avrigeanu, E. Šimečková, U. Fischer *et al.*, Phys. Rev. C **101**, 024605 (2020)

[9] M. Avrigeanu, V. Avrigeanu, P. Bém *et al.*, Nucl. Data Sheets **118**, 301 (2014)

[10] M. Avrigeanu, E. Šimečková, U. Fischer *et al.*, Phys. Rev. C **94**, 014606 (2016)

[11] E. Šimečková, P. Bém, M. Honusek *et al.*, Phys. Rev. C **84**, 014605 (2011); I. Mardor, M. Avrigeanu, D. Berkovits *et al.*, Eur. Phys. J. A **54**, 91 (2018)

[12] E. Šimečková, M. Avrigeanu, J. Mrázek *et al.*, Phys. Rev. C **104**, 044615 (2021)

[13] M. Avrigeanu, V. Avrigeanu, P. Bém *et al.*, Phys. Rev. C **88**, 014612 (2013)

[14] M. Avrigeanu, V. Avrigeanu, and A.J. Koning, Phys. Rev. C **85**, 034603 (2012)

[15] M. Avrigeanu and V. Avrigeanu, *Proceedings of the 14th International Conference on Nuclear Reaction Mechanisms Varenna, Italy, 2018*, edited by F. Cerutti *et al.*, CERN-Proceedings-2019-001 (CERN, Geneva, 2019), pp. 131; J. Phys: Conf. Ser. **724**, 012003

(2016); *ibid.* **1023**, 012009 (2018); M. Avrigeanu and V. Avrigeanu AIP Conf. Proc. No. 2076 (AIP, New York, 2019), p. 020003

[16] C. Kalbach Walker, Tech.rep., IAEA,Vienna (2010)

[17] N. Otuka, E. Dupont, V. Semkova *et al.*, Nucl. Data Sheets **120**, 272 (2014); V. V. Zerkin and B. Pritychenko, *The experimental nuclear reaction data (EXFOR)*, Nucl. Instrum. Methods Phys. Res. A **888**, 31 (2018); International Atomic Energy Agency (IAEA) Report IAEA-NDS-206, Vienna, 2008, https://www-nds.iaea.org/exfor/

[18] A. J. Koning and D. Rochman, Nucl. Data Sheets **113**, 2841 (2012); A. J. Koning *et al.*, TENDL-2021: TALYS-based evaluated nuclear data library, `https://tendl.web.psi.ch/tendl_2021/tendl2021.html`

[19] A. J. Koning, S. Hilaire, and M. C. Duijvestijn, TALYS-1.0, in *Proceedings of the International Conference on Nuclear Data for Science and Technology, April 22-27, 2007, Nice, France*, edited by O. Bersillon, F. Gunsing, E. Bauge, R. Jacqmin, and S. Leray (EDP Sciences, Paris, 2008), p. 211; v. TALYS-1.96, 2021, http://www.talys.eu

[20] I. J. Thompson, Comput. Phys. Rep. **7**, 167 (1988); v. FRES **2.9** (2011), LLNL-SM-485670, http://www.fresco.org.uk/input2.9/html/index.html

[21] Y. Iseri, M. Yahiro, and M. Kamimura, Prog. Theor. Phys. Suppl. **89**, 84 (1986)

[22] P. Guazzoni, L. Zetta, A. Covello *et al.*, Phys. Rev. C **83**, 044614 (2011)

[23] D. M. Janseitov, S. M. Lukyanov, K. Mendibayev *et al.*, Int. J. of Modern Phys. E **27**, 1850089 (2018)

[24] R. M. DelVecchio, Phys. Rev. C **7**, 677 (1973)

[25] Evaluated Nuclear Structure Data File (ENSDF), http://www.nndc.bnl.gov/ensdf/

[26] A. J. Koning and J. P. Delaroche, Nucl. Phys. A **713**, 231 (2003)

[27] W. W. Daehnick, J. D. Childs, and Z. Vrcelj, Phys. Rev. C **21**, 2253 (1980)

[28] F. D. Becchetti, Jr. and G. W. Greenlees, John H. Wiliams Laboratory Annual Report 1969 (Minnesota Univ., Minneapolis, 1969), p. 116

[29] V. Avrigeanu, P. E. Hodgson, and M. Avrigeanu, Phys. Rev. C **49**, 2136 (1994)

[30] V. Avrigeanu, M. Avrigeanu, and C. Manailescu, Phys. Rev. C **90**, 044612 (2014)

[31] A. J. Koning and D. Rochman, Nucl. Data Sheets **113**, 2841 (2012); A. J. Koning *et al.*, TENDL-2019: TALYS-based evaluated nuclear data library, `https://tendl.web.psi.ch/tendl_2019/tendl2019.html`

[32] J. Lei and A. M. Moro, Phys Rev C **92**, 044616 (2015); J. Lei and A. M. Moro, Phys Rev C **97**, 011601 (2018)

[33] K. Ogata and K. Yoshida, Phys Rev C **94** 051603 (2016)

[34] G. Potel, G. Perdikakis, B.V. Carlson *et al.*, Eur. Phys. J. A **53** 178 (2017)

[35] A. Kreisel, L. Weissman, A. Cohen *et al.*, Phys. Rev. C **99**, 034611 (2019)

[36] X. Ledoux, J. C. Foy, J. E. Ducret *et al.*, Eur Phys J A **57**, 257 (2021)